21, rue d'Artois, F-75008 PARIS
http : //www.cigre.org

CIGRE US National Committee
2021 Grid of the Future Symposium

PMU Limitations in Monitoring Fast Dynamics in Low Inertia Systems

H. HOOSHYAR, A. HADDADI, E. FARANTATOS, M. PATEL
Electric Power Research Institute
USA

SUMMARY

The continuously increasing integration of inverter-based resources (IBRs) to the grid, changes its dynamic stability and transient performance. Synchrophasors provided by Phasor Measurement Units (PMUs) due to their high-resolution and synchronized time stamping can be used to monitor these dynamics. However, the filtering and signal processing within a PMU might compromise the accuracy of the monitoring. In that case high-resolution sampled value (point-on-wave) synchronized measurements might be beneficial compared to synchrophasors. The objective of this work is to assess the performance of PMUs in accurately capturing fast grid dynamics in IBR dominated systems, depending on their class and filter parameters.

KEYWORDS

Inverter-Based Resources (IBR), Phasor Measurement Unit (PMU), Signal Processing, Filtering, Monitoring, Control

hhooshyar@epri.com

I. INTRODUCTION

Synchrophasor technology, due to the high-resolution and accurate time stamping of the measurements provided by Phasor Measurement Units (PMUs), is a technology that can be used to monitor and assess the stability of the grid in real-time. There are presently several research-grade and commercial PMU based applications that provide system security assessment [1]-[4].

Meanwhile, the continuously increasing deployment of inverter-based resources (IBRs) in power systems changes the generation mix. One of the main challenges resulting from that is the change in the dynamic behaviour of the grid and its stability characteristics, including the reduction in system inertia. IBRs exhibit different dynamic and transient behaviour compared to conventional synchronous generators (SGs) due to inherent differences between their physical components. SGs have a large rotating mass which effectively ties them to the power system with synchronizing forces and mainly defines their dynamic response to a disturbance in the power system. By contrast, IBRs may (e.g. WTGs) or may not (e.g. PV) have a rotating mass component, and the dynamic response of an IBR depends, to a large extent, on the control schemes of the inverters which can have a very fast response time. Thus, the increasing integration of IBRs in the power systems has resulted in fast grid dynamics that have not been experienced in the past.

Low levels of system inertia might jeopardize the dynamic stability performance of the grid. Thus, it is of growing R&D interest to use PMUs and synchrophasor technology to assess grid stability in inverter-dominated systems. In particular, detection and monitoring of oscillations due to IBRs is an emerging PMU application that could provide operators actionable information to ensure grid security and efficiency. While PMUs provide a potential solution to monitor these fast dynamics given their high resolution, there are limitations with respect to the accuracy of the reported synchrophasors, due to the signal processing of a PMU.

The objective of this work is to assess the performance of PMUs in accurately capturing fast grid dynamics in IBR dominated systems, depending on their class and filter parameters. This analysis also provides insights whether synchrophasors are adequate, or high-resolution point-of-wave measurements are needed. Towards this goal, in this work, a generic PMU model was developed in an EMT simulation platform. This PMU model was integrated into grid models with IBRs, and inverter instability scenarios resulting in relatively high frequency dynamics (in the sub-synchronous frequency region) were simulated. The accuracy of the reported output of the PMU was then evaluated and analysed.

The rest of the paper is organized as follows: section II gives an overview of the generic PMU model. The implementation of this model in a commercial widely used in the industry EMT simulation platform is presented in section III. In section IV demonstrating results of the output of the generic PMU model in simulations of IBR-dominated systems, are provided. Conclusions are made in section V.

II. GENERIC PMU MODEL BASED ON IEEE C37.118

There are several signal processing steps within a PMU, as shown in Figure 1. The input analog signals, measured from CTs/PTs, are first converted to digital, multiplied by the nominal frequency carrier, then filtered and then transformed to a phasor using the Cartesian to polar transformation. IEEE Standard C37.118.1-2011 [5] has the following scope, it a) defines synchrophasor or synchronized phasor measurements, frequency, and ROCOF, 2) describes time-tag and synchronization requirements and 3) specifies methods for evaluation of measurements and requirements to comply with the standard under steady state and dynamic conditions. The standard does not specify hardware, software, or a method for computing phasors, frequency, or ROCOF. The standard introduces two PMU performance classes, M class and P class, and the corresponding

dynamic performance requirements. P class is intended for applications requiring fast response such as protection applications. Whereas, M class is intended for applications that could be adversely affected by aliased signals and do not require the fastest reporting speed. The letter M is used since analytic measurements often require greater precision but do not require minimal reporting delay. The class, design, and window length (WL) of the digital LP filters as well as the PMU reporting rate (RR) have significant impact on the frequency content of the reported synchrophasor, which might become noticeably different than the frequency content of the measured signal. In addition, the WL of the digital LP filter delays the reported synchrophasors by half of its length [6], [7].

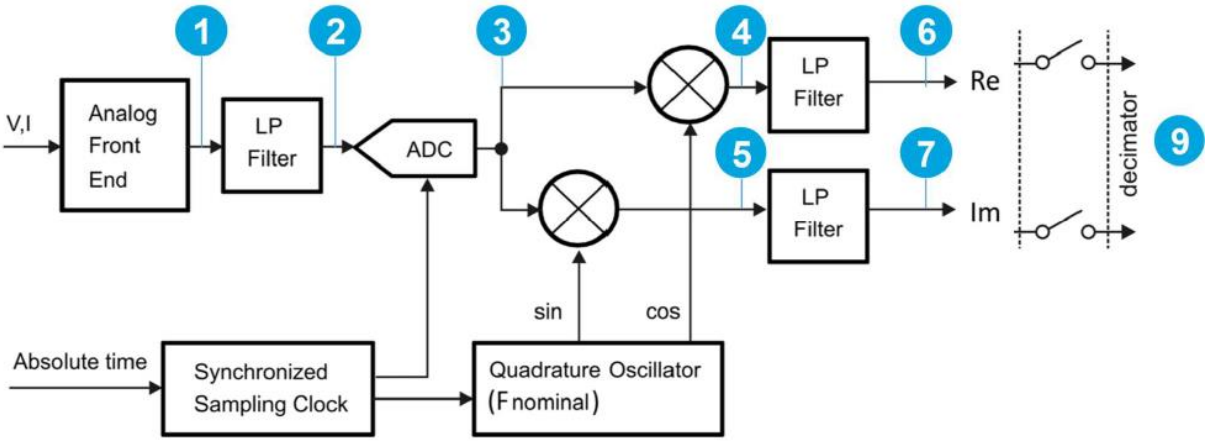

Figure 1. Signal processing model of a PMU

An analog LP filter is the first step of the PMU signal processing. It is designed to filter out high frequency noises of the input signal and limit its bandwidth to be compatible with the sampling frequency in the next step; therefore, its cut-off frequency has to be less than half of the sampling frequency. Note that the IEEE C37.118 standard is silent about the performance requirements of this filter.

The next step of the PMU signal processing is the Analog to Digital Conversion (ADC) where the signal is sampled with a high sampling frequency, e.g. 1kHz.

Once the input signal is sampled, it is multiplied by the nominal frequency carrier, that is $\cos(\omega_0 nT_s) + j\sin(\omega_0 nT_s)$ where ω_0 is the nominal frequency and T_s is the sampling interval. Assuming the sampled input signal to be $y(n) = \cos(\omega nT_s + \varphi)$, the product of its multiplication with the nominal frequency carrier can be obtained as:

$$\begin{aligned} x(n) = y(n) \times \{\cos(\omega_0 nT_s) + j\sin(\omega_0 nT_s)\} \\ = \frac{1}{2}\{\cos((\omega+\omega_0)nT_s + \varphi) + \cos((\omega-\omega_0)nT_s + \varphi)\} \\ + j\frac{1}{2}\{\sin((\omega+\omega_0)nT_s + \varphi) - \sin((\omega-\omega_0)nT_s + \varphi)\} \end{aligned}$$

The next step in the PMU signal processing is the digital LP filter which is designed to filter out the high frequency components that are added by the mathematical operations in the previous steps. The filtering is performed by convolving the input signal with the impulse response of the filter in the time domain. While the length of the input signal is equal to the time period during which the PMU is operating, the length of the filter impulse response is to be determined according to the desirable characteristics of the filter.

'Window Length' is the length of the filter impulse response in terms of 'cycles' which can be converted to number of samples by $N_{samples} = 'Window\ Length' \times \frac{F_s}{f_{nom}}$ where F_s is the sampling frequency and f_{nom} is the nominal frequency of the input signal. Once the number of samples is

known, the value of each sample can be computed using the mathematical formula of the filter impulse response.

The M-Class LP filter, as defined in the IEEE standard, is a Sinc filter windowed by a Hamming window. According to the IEEE standard, the samples in the time domain are computed using the following formula:

$$W(k) = \frac{\sin\left(2\pi \times \frac{2F_{fr}}{F_s} \times k\right)}{2\pi \times \frac{2F_{fr}}{F_s} \times k} h(k)$$

As the above-mentioned formula indicates, the filter impulse response is a function of:

- Filter window length (through *k*)
- Sampling frequency (through both F_s and *k*)
- PMU reporting rate (through F_{fr}). Note that F_{fr} is defined in the IEEE standard for all reporting rates (RR). The role of F_{fr} is basically to shape the filter impulse response such that the filter stopband starts from the Nyquist frequency, that is half of the PMU reporting rate. This is to avoid aliasing.

The P-Class LP filter, as defined in the IEEE standard, is a fixed two-cycles triangle filter. According to the IEEE standard, the samples of the impulse response in the time domain are computed using the following formula:

$$W(k) = \left(1 - \frac{2}{N+2}|k|\right)$$

Both M-Class and P-Class filters delay the input signal. The introduced delay is indeed the delay time in the step response of the filter. As the step function is the integral of the impulse function, the step response of the filter is the integral of its impulse response.

As the last step of the PMU data processing, the outputs of the LP filters are down-sampled at the PMU reporting rates.

III. PMU MODEL IMPLEMENTATION IN AN EMT TOOL

As the last step of the PMU data processing, the outputs of the LP filters are down-sampled at the PMU reporting rates.

This section presents the implementation of a generic PMU signal processing model as described in section II based on the Annex C of the IEEE C37.118.1 standard [5], in PSCAD/EMTDC [8], which is a commercial simulation platform designed for offline electromagnetic transient (EMT) simulation of power systems.

Figure 2 shows the implementation of the P-Class PMU model. The M-Class PMU implementation is similar and is not shown. The models consist of several sections, namely high frequency sampling, multiplication with the nominal frequency carrier, LP filtering, computation of positive sequence values, and computation of frequency and ROCOF.

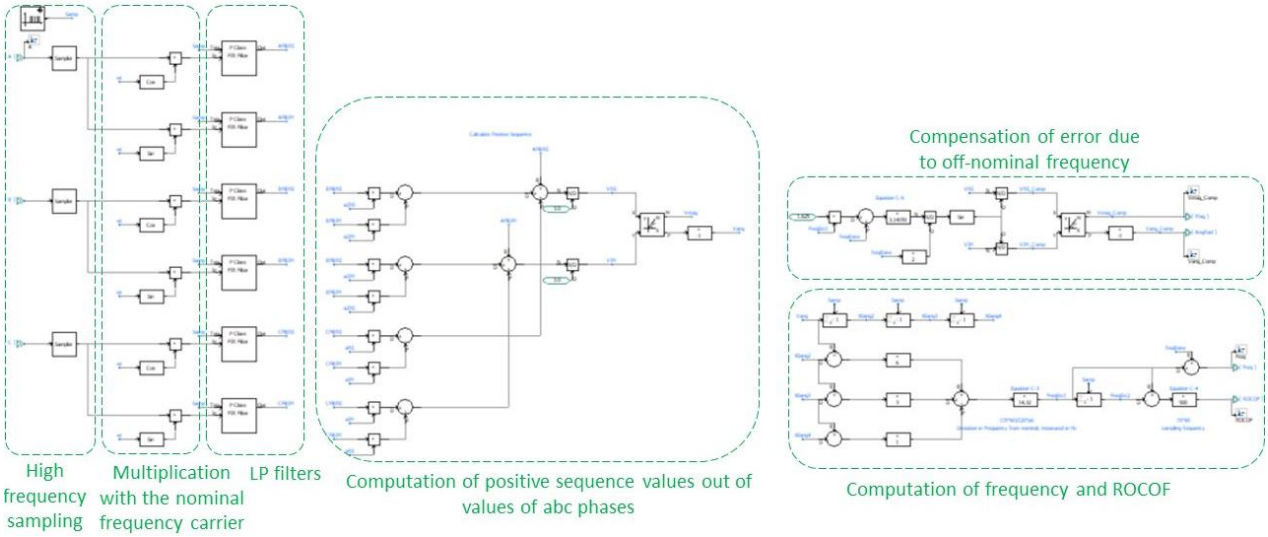

Figure 2. Implementation of P-Class PMU signal processing model

To illustrate the performance of the generic PMU models, a three-phase voltage signal, shown in Figure 3, is used as an input. Figure 4 and Figure 5 show the output of the M-Class and P-Class PMU models with respect to magnitude and phase angle.

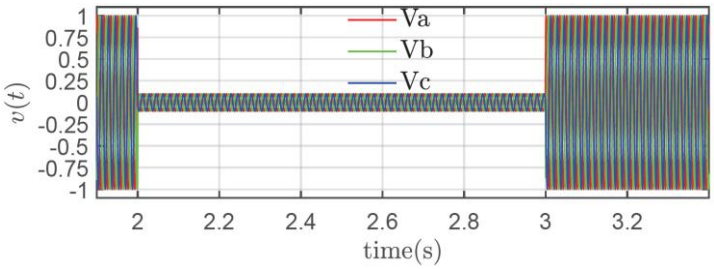

Figure 3. Three-Phase Voltage Signal for PMU Model Testing

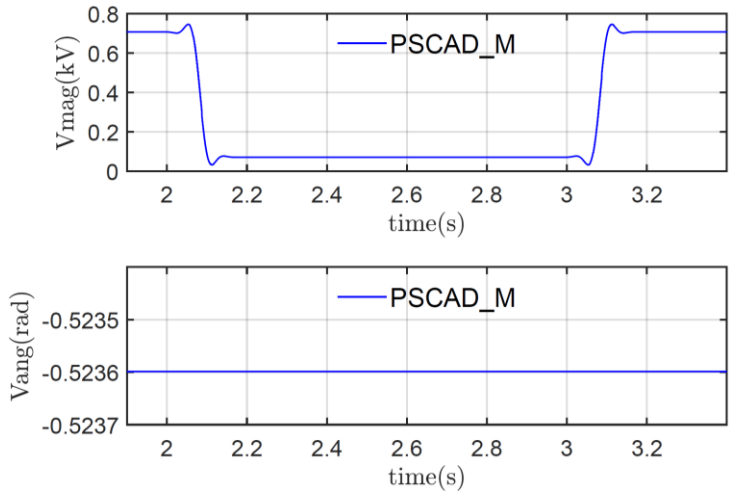

Figure 4. M-Class PMU Model Output

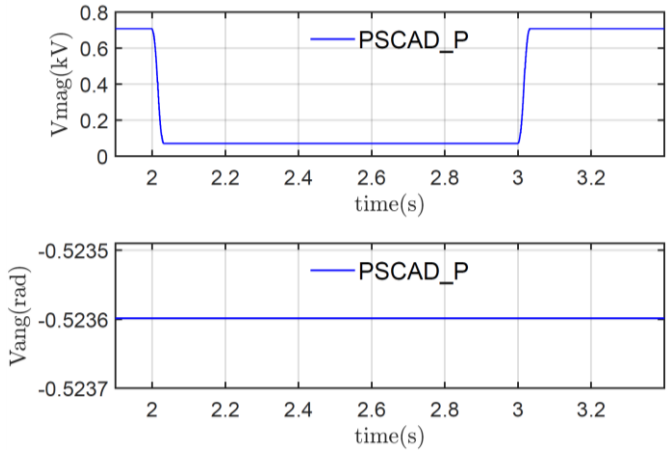

Figure 5. P-Class PMU Model Output

IV. PMU PERFORMANCE UNDER IBR-RELATED FAST GRID DYNAMICS

While PMUs provide a potential solution to monitor fast dynamics in IBR-dominated power systems, there are limitations with respect to the accuracy of the reported synchrophasors, due to the signal processing of a PMU [9]. The main factors influencing these limitations include PMU class, design, and WL of the digital LP filters as well as the PMU RR.

This section illustrates these limitations by showing the inaccuracy of the reported output of the PMU when monitoring IBR-related fast dynamics. To that end, an inverter instability event resulting in relatively high frequency dynamics was simulated [10], and the performance of the generic PMU model of sections II and III in accurately capturing these dynamics is studied.

Figure 6 shows the test system which includes a Type IV wind park on BUS1. A model of the test system has been developed in PSCAD/EMTDC environment including the generic PMU model described in section II.

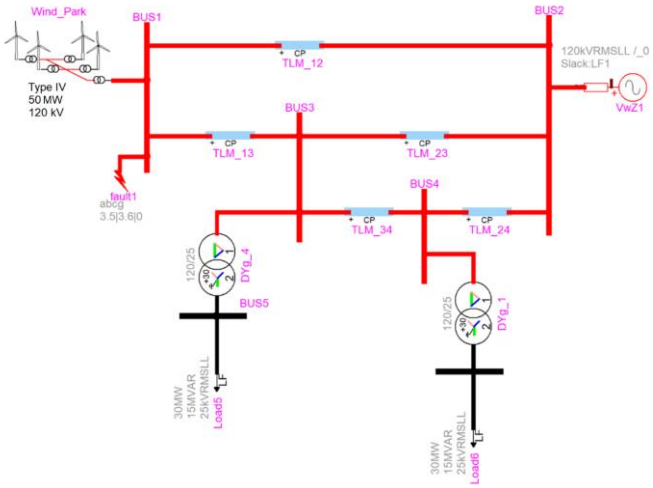

Figure 6. Test System

A temporary three-phase-to-ground fault on BUS1 followed by the outage of the line from BUS1 to BUS2 leads to an inverter instability manifesting itself as oscillations in the amplitude and phase angle of system voltages, as shown in Figure 7. The frequency of these oscillations depends on the inverter control parameters. By changing these control parameters, three oscillation frequency scenarios have been simulated:

i. Scenario 1 with an oscillation frequency of 5 Hz;
ii. Scenario 2 with an oscillation frequency of 8 Hz;
iii. Scenario 3 with an oscillation frequency of 27 Hz.

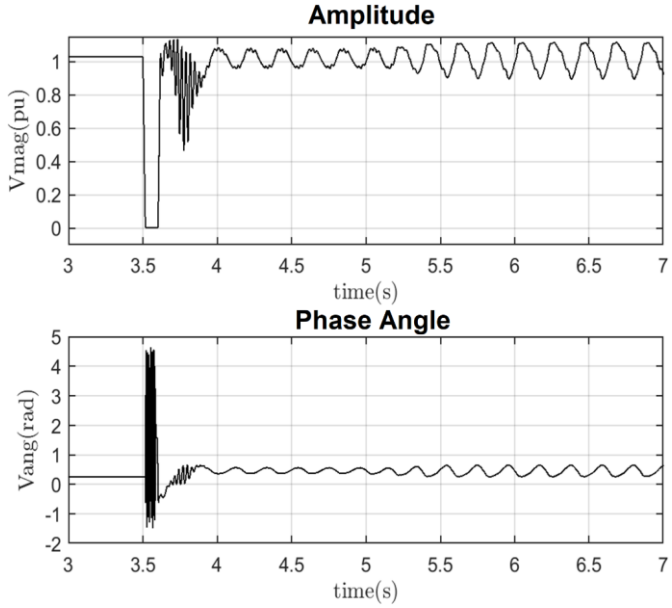

Figure 7. Simulated inverter instability caused by a three-phase fault at the terminal of an IBR followed by a line outage

The amplitude and phase angle of these oscillations have been measured using the following approaches:

1. A fast Fourier transform algorithm (FFT) which gives a full presentation of the frequency content of the signals;
2. PMU P-Class RR=60 frames per second (fps);
3. PMU M-Class WL=12 cycles RR=60 fps;
4. PMU P-Class, RR=30 fps;
5. PMU M-Class WL=6 cycles RR=60 fps;
6. PMU M-Class WL=12 cycles RR=30 fps; and
7. PMU M-Class WL=6 cycles RR=30 fps.

The results have been cross-examined to study the accuracy of the PMU-reported signals depending on the PMU class and filter parameters.

A. Scenario 1 (5Hz Oscillations)

Figure 8 compares the analytically calculated (FFT) and PMU reported amplitude and phase angle of voltage of BUS1 in this case, and Table I presents the calculated Total Vector Error (TVE) **Error! Reference source not found.**. Please note that although TVE is defined for the fundamental frequency, here, we are extending its use to examine how well the PMU has preserved the oscillations. As shown, the reconstructed PMU signals follow the measured signal, and the PMU captures the dominant 5 Hz component since the frequency is within the passband of the PMU signal processing model. The largest TVE is 3.51% corresponding to PMU P-Class RR=30 fps. The reconstructed time-domain magnitude and phase angle signals of PMUs show a time delay of approximately half of the PMU filter WL, which is expected [6], [7]. For the M-class PMU with WL=12 cycles, the delay is about 6 cycles, and for the M-class PMU with WL=6 cycles, the delay is about 3 cycles.

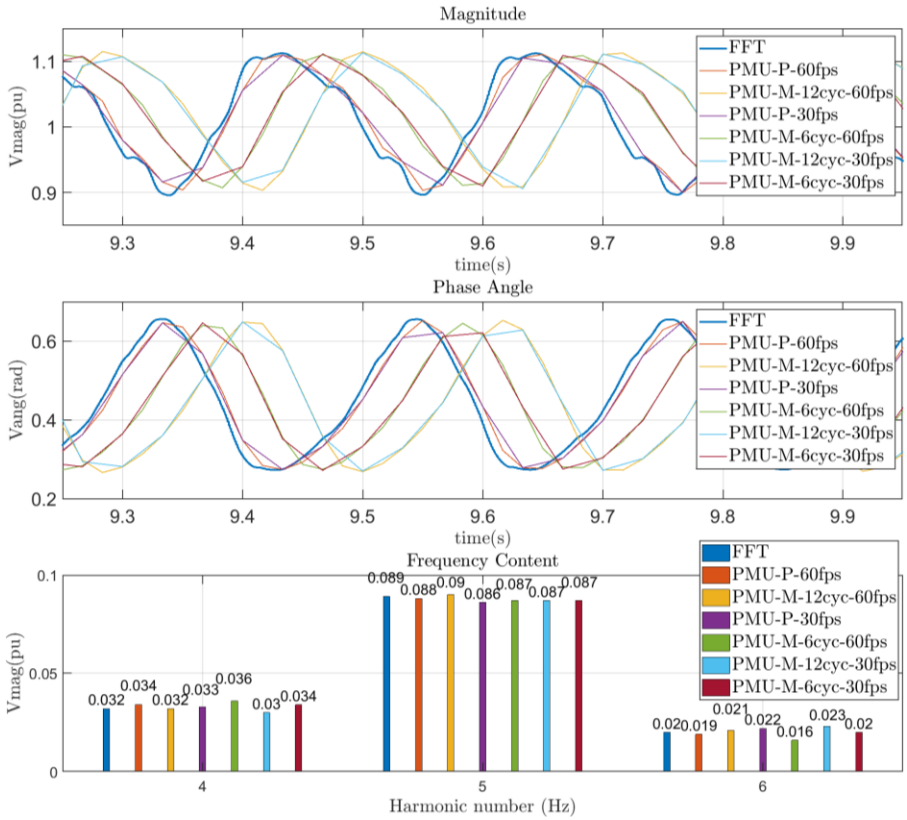

Figure 8. Analytical (FFT) vs. PMU reported amplitude and phase angle of voltage for a 5 Hz oscillation

TABLE I. Calculated Total Vector Error (TVE)

Measurement method	TVE (%)		
	5 Hz oscillation	8 Hz oscillation	27 Hz oscillation
FFT	N.A.	N.A.	N.A.
PMU-P-60fps	1.50	4.76	55.11
PMU-M-12cyc-60fps	0.13	0.03	98.07
PMU-P-30fps	3.51	14.29	N.A.
PMU-M-6cyc-60fps	2.87	9.53	94.06
PMU-M-12cyc-30fps	2.28	9.52	N.A.
PMU-M-6cyc-30fps	2.45	12.70	N.A.

B. Scenario 2 (8Hz Oscillations)

Figure 9 shows the analytical vs. PMU-reported amplitude and phase angle for the 8-Hz oscillation scenario, and Table I presents the corresponding TVE. As shown, the PMU captures the dominant 8 Hz component; however, TVE is generally increased with respect to the 5-Hz oscillation scenario. The reason is the attenuation caused by the PMU signal processing which makes the frequency content of the reported synchrophasor to become different than that of the measured signal. The largest TVE is 14.29% corresponding to PMU P-Class RR=30 fps. This is expected since the P-class generally has a lower precision than the M-class, and the lower PMU RR further deteriorates the precision [6], [7].

In conclusion, the PMU may not accurately capture faster system dynamics, depending on the class and filter parameters.

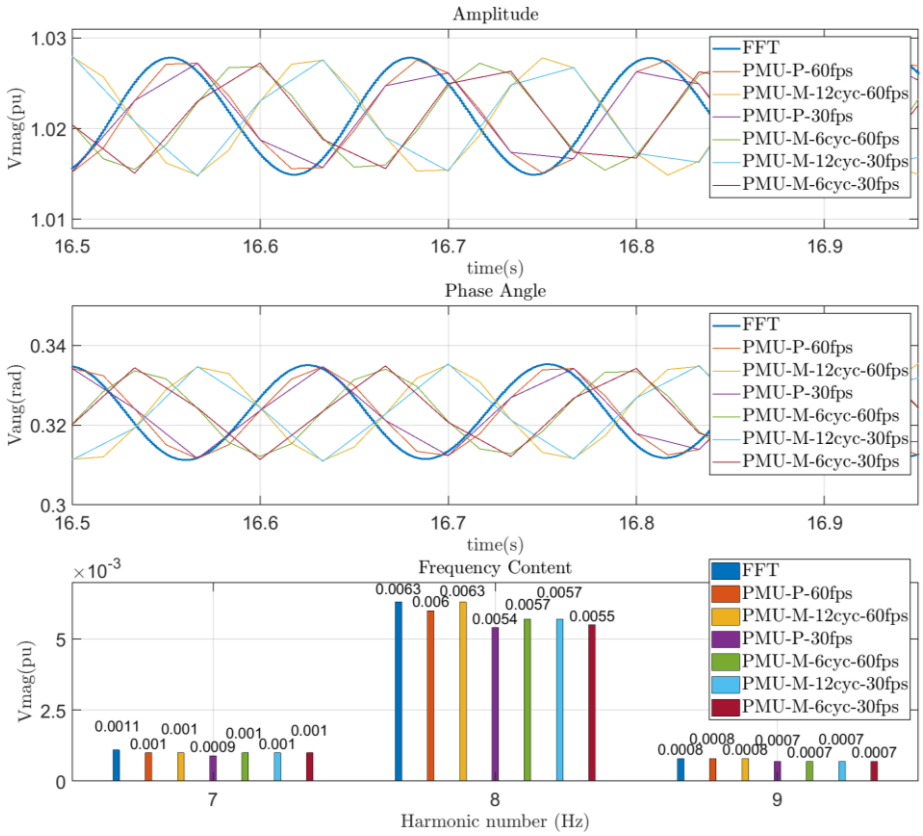

Figure 9. Analytical (FFT) vs. PMU reported amplitude and phase angle of voltage for a 8 Hz oscillation

A. Scenario 3 (27Hz Oscillations)

Figure 10 shows the analytical vs. PMU-reported amplitude and phase angle of voltage for the 27-Hz oscillation scenario, and Table I presents the corresponding TVE. As shown, the reconstructed signals do not follow the fast transients of the measured signal, and the frequency content of the reconstructed PMU-based signals becomes significantly different than that of the measured signal. TVE is also significantly increased with respect to the 5-Hz and 8-Hz oscillation scenarios. The reason is the attenuation caused by the PMU signal processing. This case further shows the decreased accuracy of synchrophasors under high frequency dynamics.

It should be mentioned that, as shown in Table I, the TVE of the 27-Hz oscillation is not reported for PMUs with 30fps due to their Nyquist frequency being 15Hz.

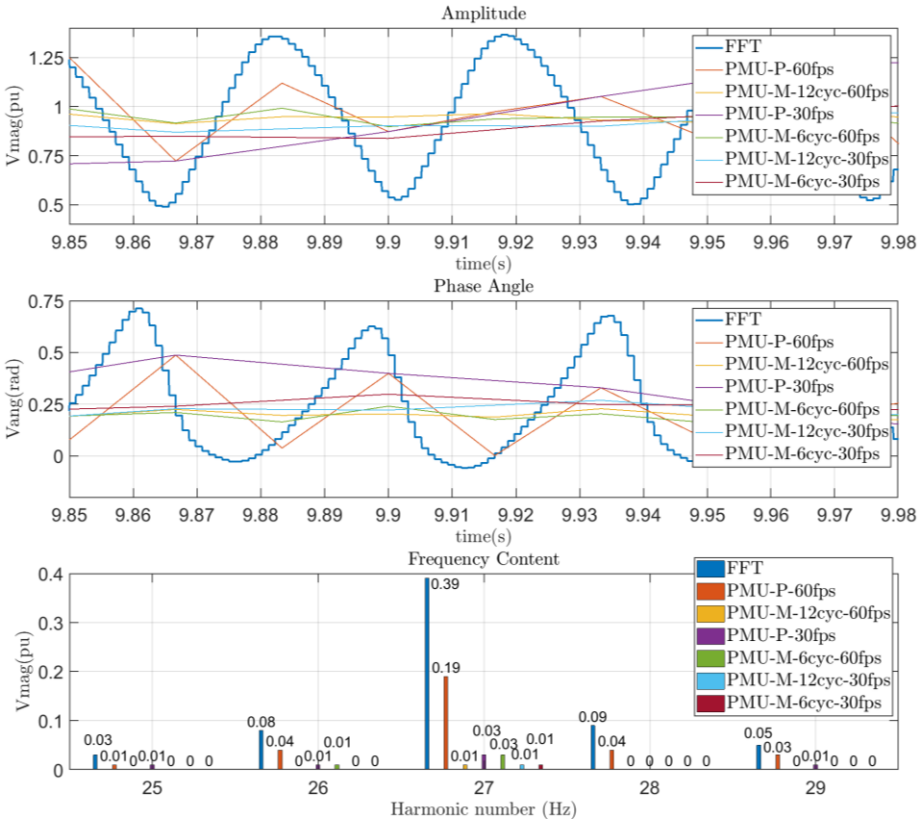

Figure 10. Analytical (FFT) vs. PMU reported amplitude and phase angle of voltage for a 27 Hz oscillation

The above case studies illustrate that synchrophasors may not be adequate to monitor fast dynamics in IBR-dominated grids. To address this limitation, a potential solution is to use high-resolution point-of-wave measurements [11].

V. CONCLUSIONS

This paper has shown that synchrophasors may not be adequate for accurately capturing fast dynamics in IBR-dominated power systems. The reason is the mathematical operation performed on the input signal by the signal processing scheme of the PMU which may cause the frequency content of the PMU output to become different than that of the input signal. The factors influencing this behavior include PMU class, design, and WL of the digital LP filters as well as the PMU RR. This report has provided examples of such limitations by showing the inaccuracy of PMU-reported amplitude of high frequency oscillations caused by inverter instability. The impact of PMU class and filter parameters on the performance has been illustrated. These limitations highlight the inadequacy of synchrophasors for grid monitoring in IBR-dominated power systems and the potential need for high-resolution point-of-wave measurements.

BIBLIOGRAPHY

[1] A.G. Phadke, J.S. Thorp, Synchronized Phasor Measurements and Their Applications, 2nd ed. Springer, 2017.

[2] ERCOT, “Synchrophasor Based Oscillation Detection in ERCOT operations”, presented at NASPI, Springfield, MA, USA, Sept. 26, 2017.

[3] ISO-NE, "Online Oscillation Management at ISO New England", presented at NASPI, Springfield, MA, USA, Sept. 27, 2017.

[4] BPA, “Synchrophasor based Oscillation Detection at Bonneville Power Administration”, presented at NERC SMS Meeting, June, 2016.

[5] IEEE C37.118.1-2011 - IEEE Standard for Synchrophasor Measurements for Power Systems.

[6] A. Goldstein, “PMU estimate error due to low-pass filter transfer function,” 2019 International Conference on Smart Grid Synchronized Measurements and Analytics (SGSMA), College Station, TX, USA, 2019, pp. 1-8.

[7] Ken Martin, Electric Power Group, “Phasor Measurements: Standards and Their Application”, IEEE Standards Association Webinar, August 2020

[8] Manitoba Hydro International, PSCAD, “https://www.pscad.com/”

[9] Recommended Disturbance Monitoring for Inverter-Based Resources, NERC SMS White Paper, November 2018.

[10] W. Wang et al., “Instability of PLL-synchronized converter-based generators in low short-circuit systems and the limitations of positive sequence modeling,” 2018 North American Power Symposium (NAPS), Fargo, ND, pp. 1-6, 2018.

[11] Abhishek Madhyasth, AMETEK Power Instruments, “Analytics with Continuous Point-on-Wave Data -A Signal Processing Perspective”, presented at NASPI, Nov. 2020